# Structural analysis and optimization of anisogrid composite lattice cylindrical shells

V.G. Belardi[a], P. Fanelli[b], F. Vivio[a,*]

[a]*Department of Enterprise Engineering - University of Rome Tor Vergata, Via del Politecnico, 1, 00133, Rome, Italy*
[b]*DEIM, University of Tuscia, Largo dell'Università, 01100 Viterbo, Italy*

**Abstract**

A structural analysis and an optimization method for anisogrid composite lattice shell structures is proposed, considering cylindrical structures simultaneously subjected to different external loads and multiple stiffness constraints. A discrete approach is used to exactly estimate the critical buckling load of the anisogrid lattice structure, independently of the buckling failure mode. The method makes use of a full FE parametric modeling technique able to manage all the geometrical parameters of the anisogrid composite lattice structure. Then an optimization procedure based on the genetic algorithm NSGA-II has been performed; it allows to analyze different alternatives in terms of geometrical variables, both continuous and discrete, driving the search towards the optimal solution in term of mass and conformity with all structural and stiffness constraints, aiming at the preliminary design of an actual structure. The practical usefulness and applicability of the proposed procedure to industrial cases was demonstrated through numerical examples where the anisogrid lattice structure was subjected to multiple external loads and stiffness constraints simultaneously applied.

*Keywords:* A. Carbon Fiber, B. Buckling, C. Finite element analysis (FEA), E. Filament winding, Genetic Algorithm Optimization

## 1. Introduction

The growing needs of lightweight and structural efficiency in aeronautic and aerospace industries brought to the development of a new design solution for grid structures: anisogrid composite lattice structures, highly capable of withstanding compression loads in conjunction with substantial stiffness features. These features allow to obtain important mass saving and cost reduction in reference to conventional aluminum components. The idea of grid structures realized with composite materials belong to Vasiliev et al. [1], initial studies on this topic took place in Russia during the early 80s with a research program that brought to the development of the first design and manufacturing methods. Successive papers about anisogrid composite lattice structures of the same authors shown progresses in this field [2, 3]: load-bearing parts such as rocket interstages, payload adapters and fuselage segments, characterized by high structural and mass efficiencies, were made by continuous filament winding which remains the most widespread fabrication technology. More recently, a new technology based on dry robotic winding of the lattice structure, followed by resin infusion under vacuum was demonstrated [4].

Anisogrid lattice structures can be found in the form of cylindrical or conical lattice shells, depending on the particular application. They are composed of a regular pattern of elementary lattice cells constructed by two systems of unidirectional composite ribs with rectangular cross-section: two sets of helical ribs, inclined with respect to the meridian curve of the shell with the same angle but in opposite directions and hoop ribs. Geometrical schemes made of hexagonal or triangular cells are normally constructed through cells' repetition alongside the meridian curve of shell and around its axis. The particular choice of the elementary lattice cell type affects the strength and the stiffness of the anisogrid lattice structure. When needed, a skin, external or internal to the ribs and co-cured with them, without important structural characteristics but with a functional role is added to the lattice shell.

Different sizing and optimization methodologies can be found in literature, which concern with cylindrical and conical lattice shells and both typologies of cells. Many of these methods consider the anisogrid lattice structure as a continuum shell and the stiffness properties of the ribs are distributed over the medium surface of the equivalent shell applying smearing techniques [5–8] meanwhile discrete approaches based on the finite element method are less common [9, 10].

The minimization of safety factors belongs to the former category of approaches and it was proposed by Vasiliev et al. for cylindrical [5] and conical shells [11]. It represents an analytical solution to the problem of constrained structural optimization of an axially compressed anisogrid composite lattice structure without an additional skin.

Totaro and Gürdal expanded this approach [6], including the axial stiffness requirement of the anisogrid lattice structure through a numerical optimization routine capable of parametrically exploring configurations with different number of helical ribs to find the solution which satisfies all constraints. Furthermore, a formulation of the local buckling coefficient which

*Corresponding author. Tel.: +39 06 72597123.
*Email address:* vivio@uniroma2.it (F. Vivio)

takes into account material and geometrical properties of the unidirectional ribs was provided for the triangular [12] and the hexagonal cell [13] permitting to better estimate the in-plane local buckling resistance.

Slinchenko and Verijenko homogenization modeling technique can give reliable stress resultants evaluations of the lattice structure, except in areas where loads and constraints are applied [7]. Similarly, Kidane et al. [14] developed an equivalent model smearing the stiffness properties of the ribs and summing them to the external skin's ones.

An alternative smearing technique is the energy-based smeared stiffener model proposed by Buragohain and Velmurugan [15]; this last allows to evaluate differences in material features between ribs and nodal points where different ribs converge being reason of higher fiber volume fraction and mechanical properties. Following, global buckling critical load is evaluated and in [16] an optimal sizing procedure is outlined based on parametric analysis.

Failure maps of the cylindrical lattice structure are derived by Zheng et al. [8] revealing that the most dangerous failure mode for large-scale cylinders under axial compression is the global buckling. A numerical optimization method is then implemented to size the structure under strength and axial stiffness constraints.

Anyway, the main limit of the continuous approaches consists in the possibility of not correctly estimate the critical buckling mode. In fact, particular buckling modes connected to the mixed shell-frame nature of the anisogrid lattice structure, which do not have a proper analytical description, can arise and provoke the failure but they are not contemplated in the continuous models.

On the other hand, the purpose of discrete approaches is to consider the lattice shell accounting for its reticulated nature, i.e. the actual one, not including equivalent stiffness properties. Usually, the employed discretization is strictly connected with the finite element method and, typically, 1D beam or 3D solid finite element models have been developed. Conversely, works based on smearing techniques make use of finite element analysis only to provide a comparison to the theory or a refinement of the results previously obtained with the continuum models.

Buragohain and Velmurugan made use of finite element analysis in combination with twenty noded 3D layered brick elements to compare the outcomes of their smeared stiffener model [15] and of their experimental studies [17].

In the experimental study of Sorrentino et al., an isogrid cylinder was realized with filament winding; the numerical simulation of the curing process was performed through a 3D solid finite element model [18].

Morozov et al. carried out the first in-depth research works on anisogrid composite lattice structures based on the application of 1D beam elements. Furthermore, an automated procedure to generate meshes was developed for both cylindrical [9] and conical [19] lattice shells. Different load cases were examined, showing the influence of structural parameters on the critical buckling load.

Lai et al. analysed six different elementary lattice cells, studying the influence of the inclination of helical ribs on the buckling failure for anisogrid cylindrical shells [10].

Nevertheless, 3D solid element models are highly computationally onerous and their application is restricted to the study of structures with a limited number of ribs or to the simulation of the manufacturing process. Otherwise, 1D beam element modeling is more attractive and allows for the comprehension and the assessment of different crucial phenomena. As Morozov et al. [9] explain, the modeling of the anisogrid lattice structure as a three-dimensional frame is a more comprehensive and accurate design instrument giving the possibility to get a greater insight of instability behavior, highlighting buckling modes that smeared models are not able to provide.

Another optimization methodology was presented in [20] where Maes et al. developed a numerical optimization workflow exploiting 2D shell elements meshes of a CAD model and a genetic algorithm.

The aim of the present paper is making use of the discrete approach to accurately evaluate the critical buckling load in the design analysis, irrespective of the particular failure mode, giving a complete and exhaustive description of the buckling failure of anisogrid lattice structures, capturing all possible buckling modes connected to a particular load condition including those that cannot be properly described through an analytical formulation and thus reliably optimize the lattice shell.

The method makes use of a full FE parametric modeling technique able to manage all the geometrical parameters of the anisogrid composite lattice structure. Then an optimization procedure based on the genetic algorithm NSGA-II has been performed; it allows to analyze different alternatives in terms of geometrical variables, both continuous and discrete, driving the search towards the optimal solution in term of mass and conformity with all structural and stiffness constraints, aiming at the preliminary design of an actual structure.

In this way, it is possible to overcome the limits proper of the continuous approaches concerning the assessment of the buckling failure (the numerical examples in Section 5 are devoted to this purpose) and those of the discrete approaches which accurately describe the structural behavior of the anisogrid lattice structure but that have been exploited with limited margins of optimization, not completely taking advantage of all their possible benefits. In fact, discrete models have not been fully coupled with an optimization technique yet and the studies conducted with these techniques have presented results showing the influence on mass amount and mechanical behavior of a single parameter's variation while the others are kept fixed. Differently, the combination of parametric modeling and a genetic algorithm allows to make simultaneous changes of all variables intended to reach the optimum.

Furthermore, the only load case treated by the continuous approaches is the axial compression and neither the discrete approaches have been employed to optimize the anisogrid lattice structure undergoing a mixed loading condition. On the other hand, the proposed procedure provides the structural optimization when different types of loads are concurrently applied and when multiple stiffness constraints are considered. Indeed, the widely required condition on axial stiffness can be added to other ones, e.g. bending stiffness.

The practical usefulness and applicability of the proposed procedure to industrial cases was demonstrated through numerical examples where the anisogrid lattice structure was subjected to multiple external loads and stiffness constraints simultaneously applied

## 2. FE parametric modeling

With the objective of optimizing the anisogrid lattice structures, a FE parametric modeling technique was developed in order to explore different design solutions for a lattice structure with assigned material properties, height $L$ and diameter $D$ (Fig. 1).

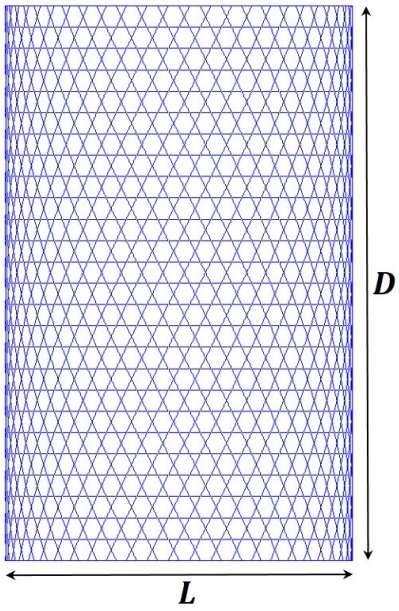


Figure 1: Cylindrical anisogrid lattice structure composed of hexagonal elementary lattice cells.

The FE parametric procedure allows to realize meshes of anisogrid lattice structures composed of hexagonal elementary lattice cells in which the hoop ribs cross halfway the helical ribs segments (Fig. 2) and it can be easily extended to the case with the triangular elementary lattice cells where the hoop ribs pass through the overlapping areas between helical ribs.

The parametric procedure is based on five variables, three of them are continuous variables (Figs. 2a and 2b) and are needed to define the cross-section's dimensions of the two kinds of ribs: the radial thickness $h$ and the widths of helical and hoop ribs, $\delta_h$ and $\delta_c$ respectively. In addition, two discrete variables, constituted by positive and integer numbers, are employed: the number of helical ribs with the same slope $n_h$ and the number of cells $N$ arranged alongside the axis of the lattice shell. This choice of geometrical variables has two strong effects on the design of the anisogrid lattice structure: firstly, the anisogrid lattice structure is manufacturable, as it consists of a finite amount of ribs and elementary lattice cells placed along its height, the second one regards the inclination angle of helical ribs $\phi$ that is converted from an optimal fixed value to an outcome parameter which is a function of the two discrete variables, which is an indispensable condition to verify any stiffness constraints.

The other geometrical parameters required to completely define a particular configuration of an anisogrid lattice structure can be extrapolated from the discrete variables: the angle between two consecutive helical ribs intersection points, Fig. 2(c):

$$\vartheta_h = \frac{2\pi}{n_h} \tag{1}$$

and the distance between hoop ribs:

Table 1: Coordinates of the points $P_1$ and $P_2$ utilized to determine the constants $C_1$ and $C_2$.

| **Layout** | **P1** | | **P2** | |
|---|---|---|---|---|
| | $\mathbf{z_1}$ | $\boldsymbol{\vartheta_1}$ | $\mathbf{z_2}$ | $\boldsymbol{\vartheta_2}$ |
| Hexagonal Cell – Extremal Hoop Ribs | 0 | $\frac{\vartheta_h}{4}$ | $\frac{a_c}{2}$ | $\frac{\vartheta_h}{2}$ |
| 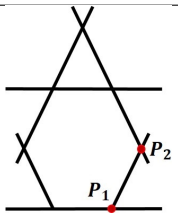 | | | | |
| Hexagonal Cell – No Extremal Hoop Ribs | 0 | 0 | $\frac{a_c}{2}$ | $\frac{\vartheta_h}{4}$ |
| 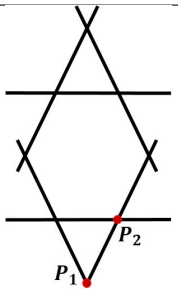 | | | | |
| Triangular Cell | 0 | 0 | $a_c$ | $\frac{\vartheta_h}{2}$ |
| 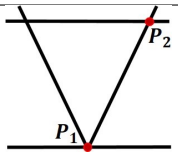 | | | | |

$$a_c = \frac{L}{2N}, \tag{2}$$

which is necessary to evaluate the height of an elementary lattice cell that is $2a_c$. Furthermore, the inclination angle of the helical ribs can be extrapolated from the discrete variables:

$$\phi = tan^{-1}\left(\frac{\pi DN}{Ln_h}\right). \tag{3}$$

Beforehand, to start the mesh generation, the first operation carried out by the FE modeler is the analytical characterization of the helical ribs mid-line. In particular, it is a geodetic curve

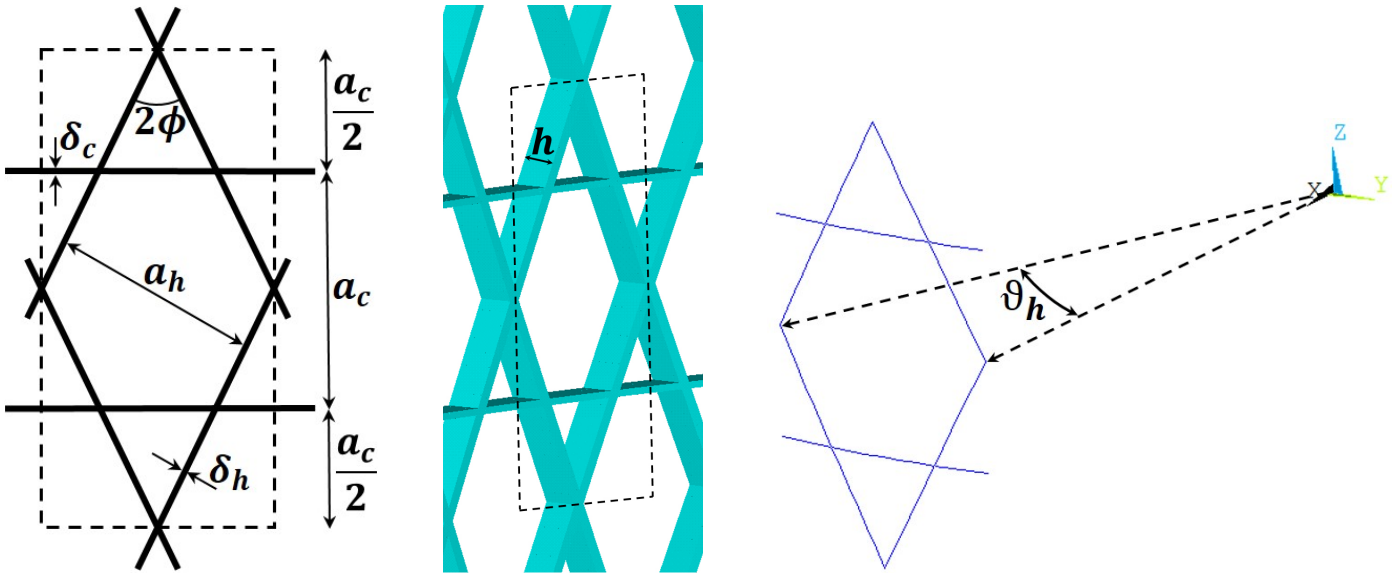


(a) (b) (c)

Figure 2: Geometry of hexagonal elementary lattice cell: (a) 2D and (b) 3D view. (c) Angle $\vartheta_h$ between two consecutive helical ribs intersection points.

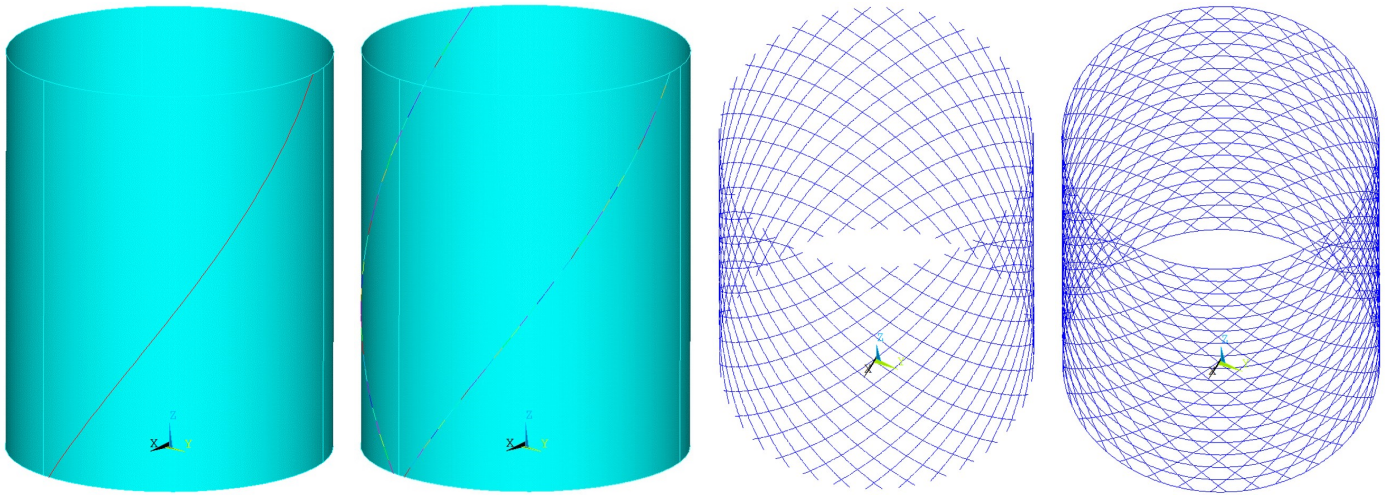

(a) (b) (c) (d)

Figure 3: (a) Geodetic curve on cylindrical surface defining the helical ribs mid-line; (b) the two geodetic curves, one for every sense of winding, after cutting; (c) mesh of helical ribs; (d) complete mesh of anisogrid lattice structure.

lying on a cylindrical surface, i.e. an helix curve as shown in Fig. 3(a). Making use of a cylindrical coordinate system with the origin at the bottom of the lattice structure and the $z$ axis coincident with its axis of symmetry, the analytical expression of the helical ribs mid-line is:

$$\vartheta = C_1 z + C_2. \tag{4}$$

This expression must be univocally defined, for the specific anisogrid lattice structure with the prescribed geometrical variables, through the identification of the coefficients $C_1$ and $C_2$ present in the equation. Taking into account two geometrical points $P_1(z_1, \vartheta_1)$ and $P_2(z_2, \vartheta_2)$ that belong to the curve, with known coordinates univocally determined by the geometric variables previously established, the coefficients becomes:

$$C_1 = \frac{\vartheta_2 - \vartheta_1}{z_2 - z_1} \qquad C_2 = \vartheta_1 - z_1 \frac{\vartheta_2 - \vartheta_1}{z_2 - z_1}. \tag{5}$$

Once the equation of the helical ribs mid-line has been determined, the procedure codified in the finite element software traces two geodetic curves, one for every verse of winding on the cylindrical surface. Afterwards, the two geodetic curves are cut to find the positions of the intersection points between two helical ribs and between an helical rib and an hoop rib, the result is shown in Fig. 3(b). This is necessary to force the successive

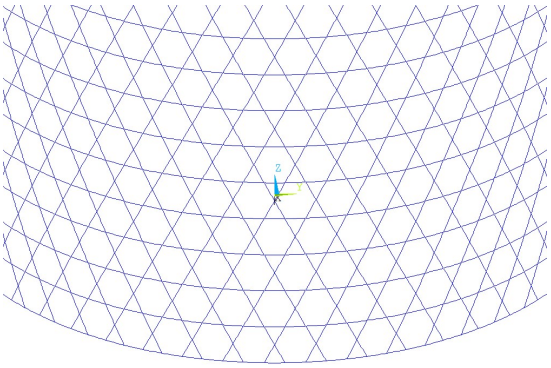

(a)

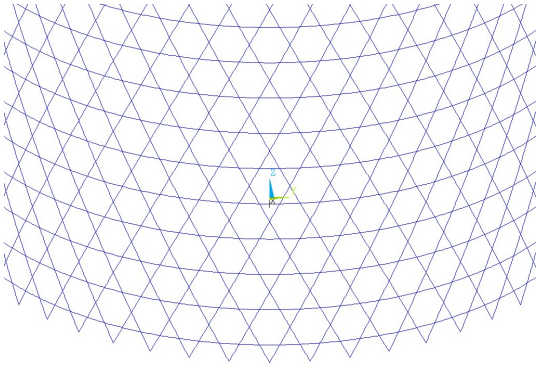

(b)

Figure 4: Configurations of anisogrid lattice structure consisting of hexagonal elementary lattice cells delimited by: (a) extremal hoop ribs and (b) overlapping areas between helical ribs.

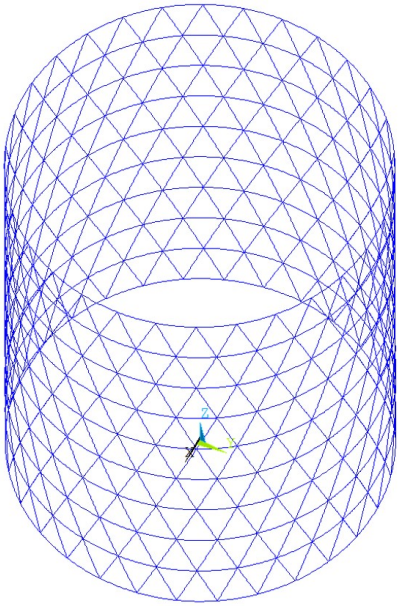

Figure 5: Mesh of anisogrid lattice structure with triangular cells.

generation of elements' nodes in correspondence of these geometrical points. This operation is carried out by means of a series of cuts executed with a geometrical plane orthogonal to the axis of the lattice shell. The geometrical plane is initially located at the vertical coordinate $z = a_c/2$ and after every cut it is moved ahead, along the $z$ axis, of a quantity $a_c/2$ until the cut sequence is completed.

The curves obtained cutting the two geodetic curves are copied $n_h$ times around the axis of the lattice structure with an angular step of $\vartheta_h$. All these lines are meshed with two noded beam element, having six degrees of freedom per node (Fig. 3c). To conveniently reproduce the twist proper of the helical rib's cross-section alongside its mid-line, the beam element's coordinate system is adjusted making use of the orientation node that is positioned on the axis of the anisogrid lattice structure. In this way, the width of the helical rib's cross-section remains perpendicular to the radius of the shell along the length of helical rib mid-line.

After that, a set of $n_c$ circumferences is drawn in the positions of hoop ribs: the first one is realized at $z = 0$, the others have a shift of $a_c$ from the previous one in the $z$ direction. Each circumference is composed of circular segments with angular extension equal to $\vartheta_h$ so that they can be enclosed between two geometrical points of intersection with helical ribs previously determined. Following, the curves constituent the hoop ribs are meshed completing the anisogrid lattice structure mesh as reported in (Fig. 3d).

Subsequently, the FE modeler computes the mass of the lattice shell evaluating the contributions of the helical ribs:

$$M_h = 2n_h \frac{L}{cos\phi} h\delta_h\rho_h \tag{6}$$

and the one related to the hoop ribs:

$$M_c = n_c\pi Dh\delta_c\rho_c, \tag{7}$$

$\rho_h$ and $\rho_c$ are the mass densities of helical and hoop ribs, respectively. The number of hoop ribs $n_c$ depends on the number of elementary lattice cells alongside the axis of the anisogrid structure: $n_c = 2N + 1$. The total mass is obtained summing up the two expressions:

$$M = M_h + M_c. \tag{8}$$

Moreover, it should be noted that the particular choice of the two geometrical points $P_1$ and $P_2$, whose coordinates are outlined in Table 1, permits to realize two different structure layouts with hexagonal elementary lattice cells: the one described up to now, delimited by extremal hoop ribs helpful to consider the presence of the end rings in Fig. 4a, and the one which ends with the overlapping areas between helical ribs, Fig. 4b. For the second layout, the first circumference necessary to generate the hoop ribs is positioned at $z = a_c/2$, meanwhile their number is $n_c = 2N$.

The parametric modeling technique employed offers the opportunity of easily realizing anisogrid lattice structures composed of triangular elementary lattice cells (Fig. 5). The coordinates of the geometrical points $P_1$ and $P_2$ for this arrangement is illustrated in the third row of Table 1, the distance between two consecutive hoop ribs becomes: $a_c = L/N$ and for this configuration the number of hoop ribs is $n_c = 2N + 1$.

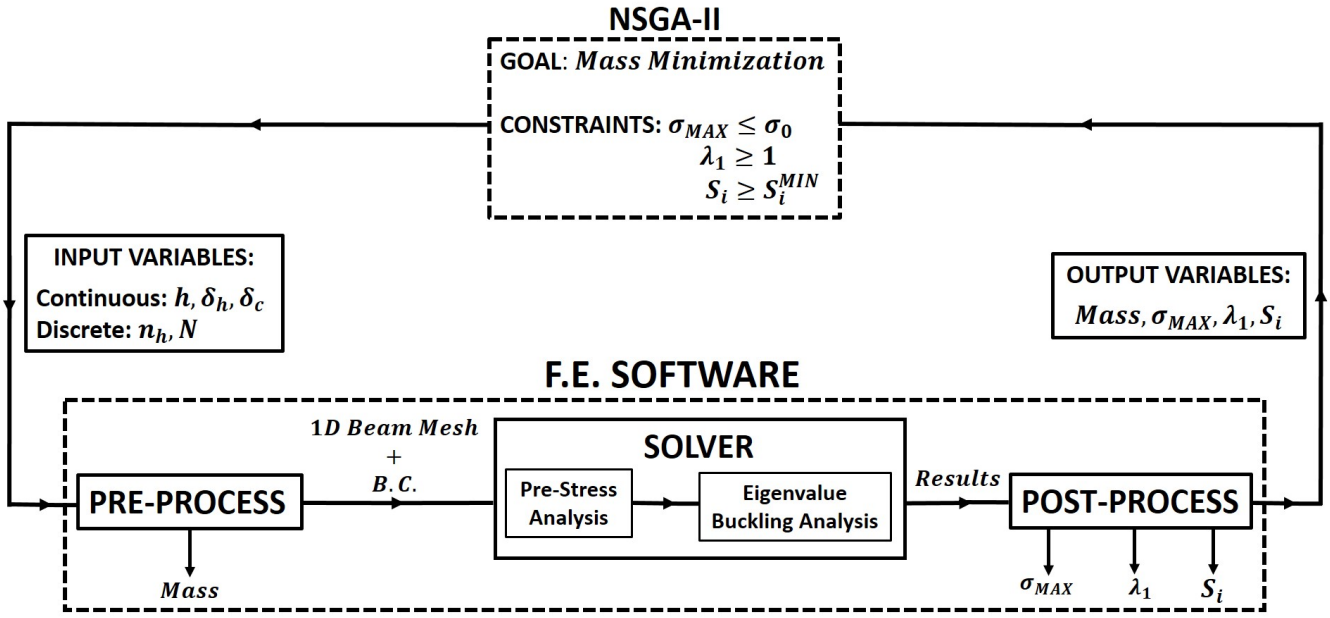


Figure 6: Logical workflow of the optimization procedure based on the finite element method coupled with the genetic algorithm NSGA-II.

## 3. Structural optimization using the NSGA-II

The design strategy for structural optimization makes use of an automatic process based on the coupling of the FE parametric procedure and the genetic algorithm NSGA-II. This last allows to deal with constrained multi-objective optimization problems involving discrete and continuous variables. For this work it is used to reach a single objective, i.e. mass minimization.

The NSGA-II provides the optimal solution ensuring the validity of a fixed number of conditions formulated as inequalities, i.e. constraints, which must be verified to accept a particular sample as a feasible solution which contributes to the attainment of the optimum. The constraints employed for the optimization of anisogrid lattice structures state:

- Material compressive strength

$$\sigma_{MAX} \leq \sigma_0;$$

- Buckling resistance

$$\lambda_1 \geq 1;$$

- Minimum level of stiffnesses

$$S_i \geq S_i^{MIN}.$$

The first imposed condition concerns the material failure and it involves only the helical ribs, stating that their maximum compressive stress $\sigma_{MAX}$ must not exceed material compressive strength $\sigma_0$. Indeed, the axial force agent on the anisogrid lattice structure is responsible of a compression stress state for helical ribs and a general traction stress state for hoop ribs. Being the material strength larger in traction than in compression, and the stress level reached by helical ribs higher than the hoop ribs' one, this last is not taken into account. Moreover, manufacturing imperfections could be reason of an elliptical cross-section of the lattice shell and consequently decrease the critical buckling load; the general tension stress state of hoop ribs neutralizes this problem recovering the circular shape for the lattice shell's cross-section. Hence, no knock-down factor for the critical buckling load due to geometrical imprecisions is needed in designing anisogrid lattice structures [1].

To complete the requisites on structural strength, the capability of preventing buckling occurrence must be added to the conditions prescribed to the optimization algorithm. The analytical approaches offer a buckling strength prevision affected by the intrinsic limit deriving from supposing only two modes as responsible of buckling failure. Indeed, these methods consider the structure as if it could only behave in two different and extremely distinct ways: as a continuum shell whose buckling response can be treated with orthotropic shell's relationships or as a three-dimensional frame, which can undergo local instability. In many cases, actually, the anisogrid lattice structure does not exhibit a well defined mechanical behavior ascribable to an orthotropic shell or to a beam framework. More frequently, it is a composition of them and the lattice structure shows buckling failure modes that are connected with its dual nature and that are characterized by the presence of lobes distributions along and around the axis of the shell. Besides, equations developed with smearing techniques to evaluate the critical buckling load are not capable to capture these types of collapse. Therefore, sometimes the correlated optimization methodologies overestimate the buckling resistance, giving as output geometrical dimensions for the lattice shell unable to fulfill the structural requirements and that consequently do not represent a reliable

design solution. Hence, the re-examination of the project is needed and it could produce an exaggerated mass addition.

To overcome these limits, the discrete approaches are needed to get the correct estimation of the buckling resistance and the instability requirement must be formulated regardless of the particular buckling failure mode. In the proposed procedure, this is achieved making use of a constraint which imposes that the first eigenvalue $\lambda_1$ computed through finite element analysis must be at least unitary. In this way, the condition on buckling strength is expressed in the most general manner encompassing all possible modes, including the local and global ones and those without a simplified theoretical formulation.

The proposed optimization methodology is highly general and further constraints concerning structural stiffness can be settled. Taking as an example the design of a rocket interstage, it must possess a controlled flexibility in order to be compliant with the guide systems of the launcher. Subsequently, some minimum level of stiffnesses parameters could be demanded to the output design. The genetic algorithm affords this requirement similarly to the others, i.e. the values are deduced by the finite element analysis and supplied to the NSGA-II which compares it with the reference values.

An extension range must be defined for the five variables, imposing their minimum and maximum values. The combination of all allowable values defines the design space where the NSGA-II operates. In this phase, some requisites regarding the manufacturing process can be introduced, such as those about ribs width which is a multiple of the fiber one.

To start the optimization process, a design of experiments (DOE) is needed. A DOE produces an initial population of samples whose purpose is providing an assessment of the structural response of the anisogrid lattice structure to the genetic algorithm, and consequently starting the automatic generation of samples. In this regard, the most widespread exploration of the design space is important to guarantee the identification of the optimal design. The Uniform Latin-Hypercube DOE has been used in order to obtain an initial population characterized by a uniform and random distribution of the samples in the design space.

The procedure utilized to optimize the design of the anisogrid lattice structure follows the logical workflow shown in Fig. 6. During the computing loops, the genetic algorithm NSGA-II supplies the finite element software with a set of geometrical variables written in a file which acts as input for the finite element software. Once input variables have been defined, the procedure calls for a batch file needed to manage the finite element analysis. Its pre-processor constructs the mesh of the anisogrid lattice structure according to the sequence of operations previously described and computes its mass $M$. In the subsequent step, boundary conditions are introduced in the model: the bottom end is fixed; nodes of the upper extremal hoop rib are connected through a set of rigid links (shown in Table 2) to the one present in its geometrical center, free from displacement constraints, where external loads are applied.

Then, finite element eigenvalue buckling analysis is carried out identifying the output variables that must be furnished to the NSGA-II to check the conformity with constraints. The anisogrid lattice structure's mass $M$, the highest compressive stress $\sigma_{MAX}$, the first eigenvalue $\lambda_1$ and stiffness values $S_i$ are recorded in an output file and acquired by the genetic algorithm, closing the loop. With this information, it deduces the set of input variables for the following iteration. The process goes on until all the samples have been analyzed.

Finally, the design which satisfies all the constraints conditions with the lowest mass is the optimal solution.

## 4. Numerical results

The optimal solutions for the design of anisogrid lattice structures subjected to different load typologies and multiple stiffness requirements are here considered. These examples are presented with the aim to validate the effectiveness and the accuracy of the proposed optimal design method and the broad potentialities of the NSGA-II, in particular when various external loads act simultaneously on the lattice shell.

The starting case-study involves a loading condition of axial compression and, in addition, a minimum axial stiffness must be assured. Nevertheless, operating conditions can consist of a mixed set of loads, so the subsequent case-studies are obtained taking into account the presence of further loads and stiffness constraints. One load condition and stiffness constraint at a time will be considered and superimposed to the first load case and then, the anisogrid lattice structure accordingly sized. Overall, four load cases were analyzed, represented in Table 2.

Object of the analyses considered in the load cases hereafter presented is a cylindrical anisogrid lattice structure consisting of hexagonal elementary lattice cells with extremal hoop ribs, diameter $D = 4$ and height $L = 7$ m. The lattice shell's material employed in the following analyses is carbon-epoxy, it is the same for both helical and hoop ribs and its properties are: Young modulus $E = 100$ GPa, compressive strength $\sigma_0 = 450$ MPa and mass density $\rho = 1,500$ Kg/m$^3$.

Aiming at a high level of generality, a wide design space was utilized to perform the analyses of the following case-studies. The minimum and maximum values of the geometrical variables used in the FE parametric modeling procedure are listed in Table 3; the design space consists of all their possible combinations.

Table 3: Range variation of problem's variables defining the design space.

| | $h$ [mm] | $\delta_h$ [mm] | $\delta_c$ [mm] | $n_h$ | $N$ |
|---|---|---|---|---|---|
| MIN Value | 13 | 2.3 | 2.3 | 65 | 20 |
| MAX Value | 35 | 18 | 18 | 140 | 50 |

### 4.1. Compression axial load and axial stiffness constraint (LC1)

The anisogrid lattice structure with dimensions and material properties earlier assigned must be designed to withstand the axial load $P = 11$ MN with a further requirement: it has to guarantee a minimum axial stiffness $S_A = 370$ MN/m. This

Table 2: The four load cases and their loading conditions and stiffness constraints.

| **Load Case 1 (LC1)** | **Load Case 2 (LC2)** | **Load Case 3 (LC3)** | **Load Case 4 (LC4)** |
|---|---|---|---|
| **Loading Conditions** | | | |
| Axial Compression | Axial Compression<br>Transverse Bending Force | Axial Compression<br>Bending Moment | Axial Compression<br>Torque Moment |
| **Stiffness Constraints** | | | |
| Axial Stiffness | Axial Stiffness<br>Transverse Bending Stiffness | Axial Stiffness<br>Bending Stiffness | Axial Stiffness<br>Torsional Stiffness |
| 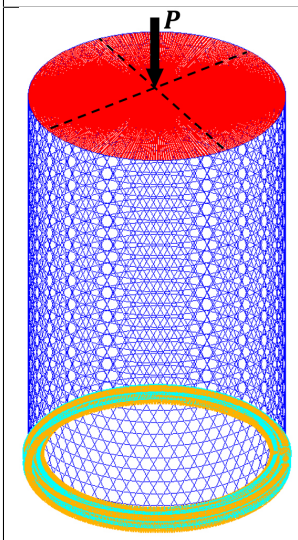 | 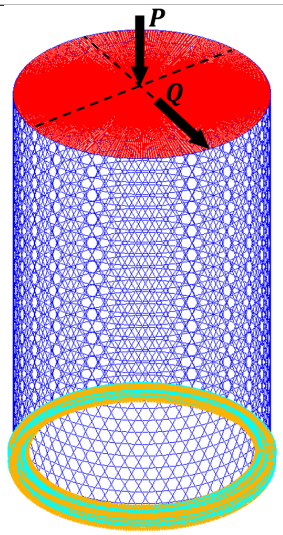 | 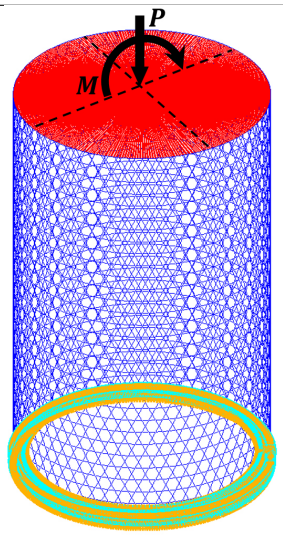 | 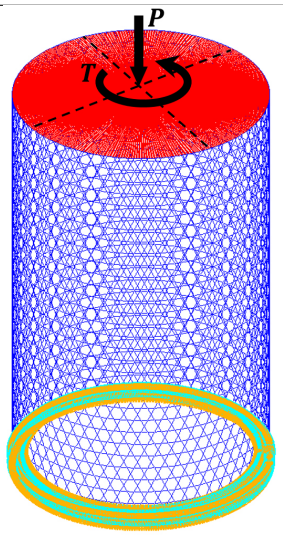 |

parameter is evaluated through the ratio between the applied load $P$ and the maximum axial displacement in the $z$ direction $u_z^{MAX}$.

The minimum mass design which concurrently satisfies the structural conditions on the maximum compressive stress, buckling resistance and restricted axial deformability was determined through the application of the FE parametric modeling technique and the genetic algorithm; results concerning the geometric variables and the structural performances can be found in Table 4.

This case-study is useful for the explanation of the physical meaning of the discrete variables. In fact, the anisogrid lattice structure can be considered as a series of $N$ circular-springs coaxial with the lattice shell and disposed along its axis, a reduction of this variable contributes to raise its axial stiffness; on the other hand, an increase of this parameter is responsible of a higher flexibility. Besides, the number of helical ribs $n_h$ has a direct influence on the stiffness of a single individual circular-spring.

The limiting conditions for this design, which drove the sizing of the lattice shell, turned out to be the buckling and stiffness constraints, that are strictly verified. Unlike, the safety factor concerning the other failure mode connected to helical ribs compressive strength is about 1.56.

The collapse of the lattice shell is due to a buckling failure mode, reported in Fig. 7, characterized by the presence of 10 vertical series of lobes and each one consists of 10 lobes. Their amplitude is more accentuated in the central zone of the anisogrid lattice structure meanwhile it decreases moving towards the extremal hoop ribs because of the clamping effect due to the boundary conditions and to the set of rigid links.

### *4.2. Transverse bending force and transverse bending stiffness constraint (LC2)*

In this case-study, the basic compression load case beforehand discussed is expanded through the application of a transverse bending force $Q = 0.5$ MN (along the $x$ axis of the model) to the upper extremal end of the lattice shell. Likewise, a second stiffness constraint is further imposed demanding a minimum transverse bending stiffness $S_{TB} = 30$ MN/m; it is defined as the ratio of the transverse bending force and the maximum displacement alongside its direction of application, i.e. $u_x^{MAX}$.

Table 5 lists the results of the optimization performed with the NSGA-II. The presence of the double external load and stiffness conditions increased the mass of 25.19% with respect to the previous case-study involving only axial compression force and axial stiffness constraint.

Concerning to ribs cross-section's dimensions, the thickness $h$ and helical ribs' width $\delta_h$ are greater than those of the preceding sizing, while hoop ribs' width $\delta_c$ is practically unchanged. Both discrete variables $n_h$ and $N$ are reduced to assure the validity of the required minimum values of stiffness.

Once again, the constraint on compressive strength resistance is amply fulfilled, indeed the associated safety factor is 1.56 as

Table 4: Geometric parameters and finite element analysis results of the anisogrid lattice structure designed under axial compression load and axial stiffness constraint.

| $M$ [Kg] | $h$ [mm] | $\delta_h$ [mm] | $\delta_c$ [mm] | $\phi$ [°] | $n_h$ | $N$ | $\sigma_{MAX}$ [MPa] | $\lambda_1$ | $u_z^{MAX}$ [mm] | $S_A$ [MN/m] |
|---|---|---|---|---|---|---|---|---|---|---|
| 563.2 | 26.66 | 6.70 | 2.33 | 25.25 | 118 | 31 | 288.38 | 1.002 | 29.72 | 370.12 |

Table 5: Geometric parameters and finite element analysis results of the anisogrid lattice structure designed under axial compression and transverse bending loads in conjunction with axial and transverse bending stiffness constraints.

| $M$ [Kg] | $h$ [mm] | $\delta_h$ [mm] | $\delta_c$ [mm] | $\phi$ [°] | $n_h$ | $N$ |
|---|---|---|---|---|---|---|
| 705.1 | 30.78 | 11.24 | 2.30 | 23.65 | 82 | 20 |
| $\sigma_{MAX}$ [MPa] | $\lambda_1$ | $u_z^{MAX}$ [mm] | $S_A$ [MN/m] | $u_x^{MAX}$ [mm] | $S_{TB}$ [MN/m] | |
| 289.15 | 1.033 | 22.62 | 486.3 | 16.66 | 30.0 | |

Table 6: Geometric parameters and finite element analysis results of the anisogrid lattice structure designed under axial compression and bending loads in conjunction with axial and bending stiffness constraints.

| $M$ [Kg] | $h$ [mm] | $\delta_h$ [mm] | $\delta_c$ [mm] | $\phi$ [°] | $n_h$ | $N$ |
|---|---|---|---|---|---|---|
| 642.2 | 30.25 | 8.02 | 3.04 | 24.39 | 99 | 25 |
| $\sigma_{MAX}$ [MPa] | $\lambda_1$ | $u_z^{MAX}$ [mm] | $S_A$ [MN/m] | $rot_y^{MAX}$ [rad] | $S_B$ [MNm/rad] | |
| 319.87 | 1.006 | 24.80 | 443.55 | $3.39 \cdot 10^{-3}$ | 884.96 | |

Table 7: Geometric parameters and finite element analysis results of the anisogrid lattice structure designed under axial compression and torsional loads in conjunction with axial and torsional stiffness constraints.

| $M$ [Kg] | $h$ [mm] | $\delta_h$ [mm] | $\delta_c$ [mm] | $\phi$ [°] | $n_h$ | $N$ |
|---|---|---|---|---|---|---|
| 677.1 | 27.18 | 6.92 | 2.32 | 28.31 | 130 | 39 |
| $\sigma_{MAX}$ [MPa] | $\lambda_1$ | $u_z^{MAX}$ [mm] | $S_A$ [MN/m] | $rot_z^{MAX}$ [rad] | $S_T$ [MNm/rad] | |
| 319.97 | 1.006 | 29.72 | 370.12 | $5.42 \cdot 10^{-3}$ | 553.51 | |

for the previous load case. Similarly, the axial stiffness $S_A$ is 31.43% higher than the minimum value. Conversely, the constraints on buckling failure mode and transverse bending stiffness resulted being the most stringent for the sizing.

The buckling failure mode of this load case, as shown in Fig. 8, makes the structure to buckle more locally, in a confined region, if compared with the previous one. The instability interests the area where the compressive stress state of the helical ribs due to the transverse bending force and axial compression are superimposed.

### *4.3. Bending force and bending stiffness constraint (LC3)*

The anisogrid lattice structure undergoes the action of the axial compression force and of the bending moment $M = 3$ MNm applied to the top of the lattice shell (along the $y$ axis of the model). Additionally, the stiffness constraint concerning axial stiffness was considered along with a constraint on bending stiffness, a minimum value of $S_B = 875$ MNm/rad was requested. This last stiffness value is evaluated through the ratio of the bending moment and the consequent angle of rotation $rot_y^{MAX}$ experienced by the upper cross-section of the lattice shell.

The application of the optimization methodology produced the outputs reported in Table 6. The mass of the lattice shell increased of 14.03% with respect to the baseline configuration of the first load case. Both discrete variables decreased and contextually the cross-sections of the two kinds of ribs present increased dimensions.

The condition on buckling failure was again a driver for the sizing of the anisogrid structure, as $\lambda_1$ is very close to the unity; likewise, the value obtained for $S_B$ strictly respects the condition for this parameter. The axial stiffness $S_A$ is the 19.88% greater than the limit value. Once again the compressive strength of helical ribs is not a critical condition being the safety factor for the failure mode induced by the compressive stress 1.41.

The buckling failure of the anisogrid lattice structure took place in the half where the bending moment causes a compression stress state of the helical ribs. The buckling mode, as shown in Fig. 9, is characterized by 3 main vertical series of lobes composed of 9 lobes. The lobes of the central strip have a bigger amplitude whit respect the other two and it progressively decreases towards the extremal hoop ribs.

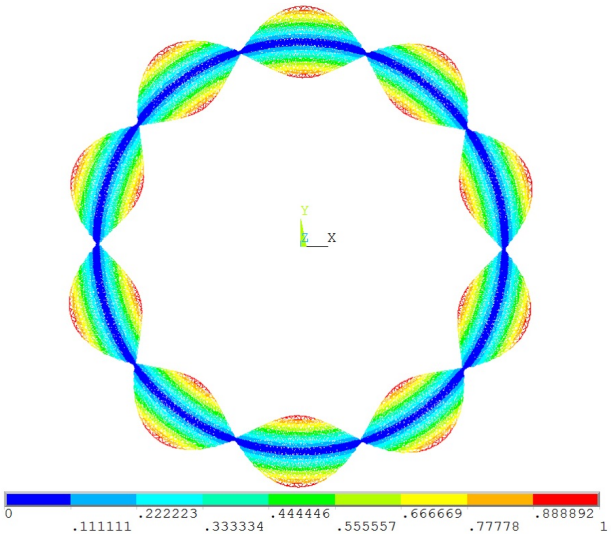


(a)

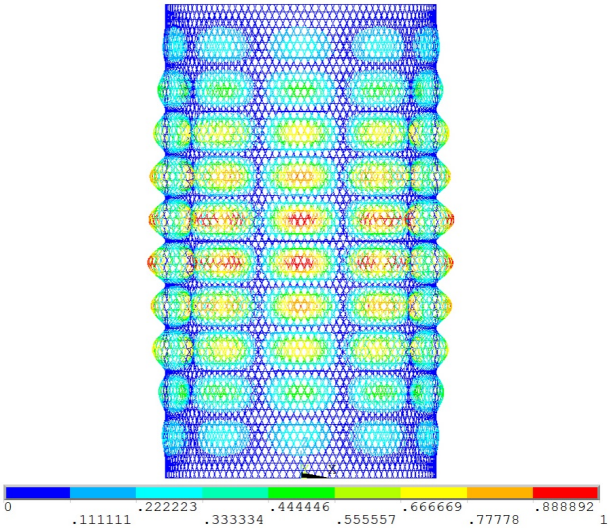


(b)

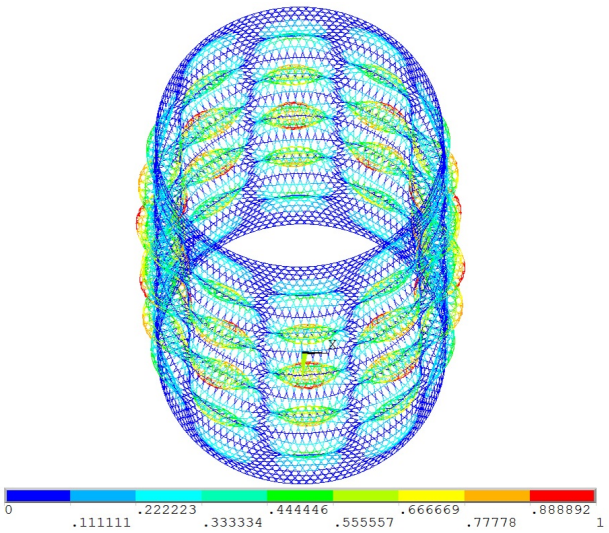


(c)

Figure 7: Buckling failure mode under the action of axial compression (LC1), $\lambda_1 = 1.002$. (a) Top view, (b) front view and (c) prospective view.

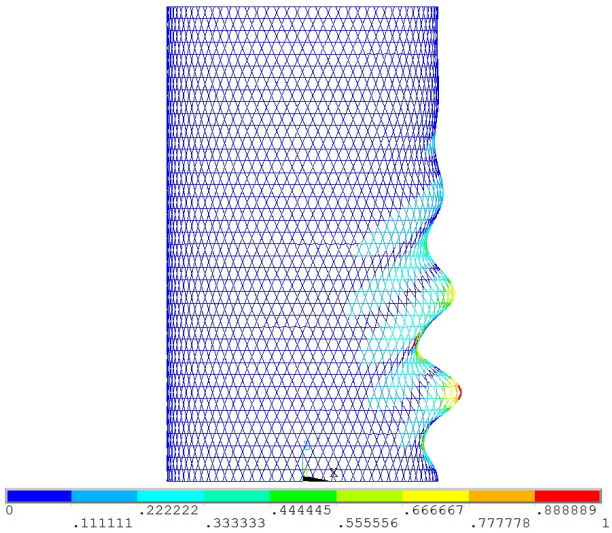


(a)

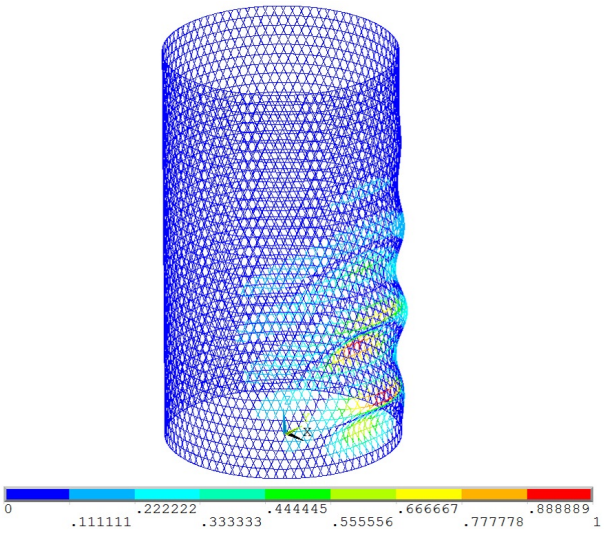


(b)

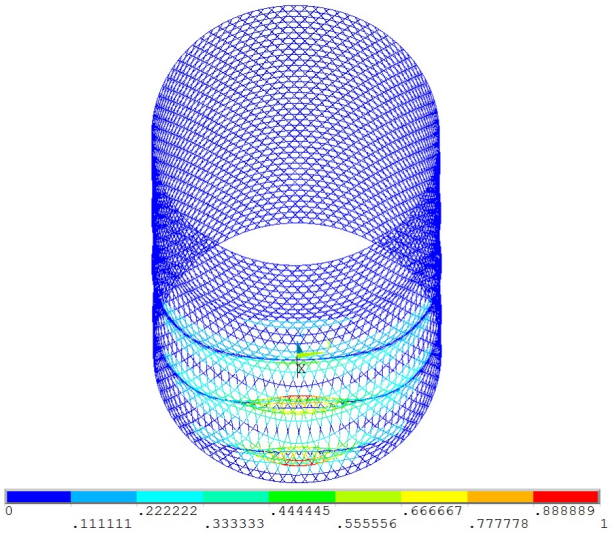


(c)

Figure 8: Buckling failure mode under the action of axial compression and transverse bending forces (LC2), $\lambda_1 = 1.033$. (a) Front view, (b) and (c) prospective views.

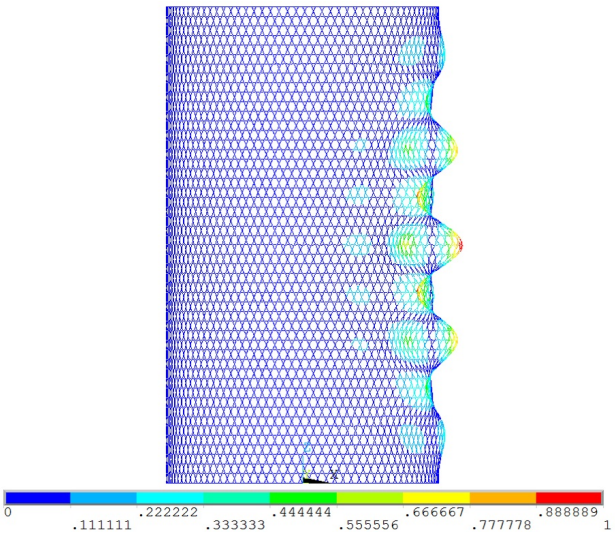


(a)

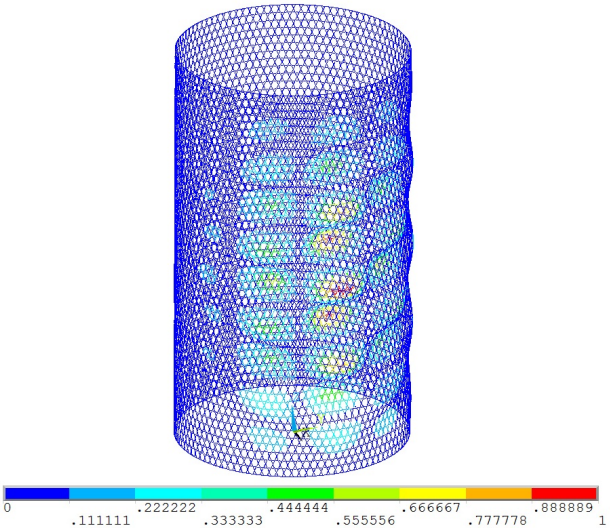


(b)

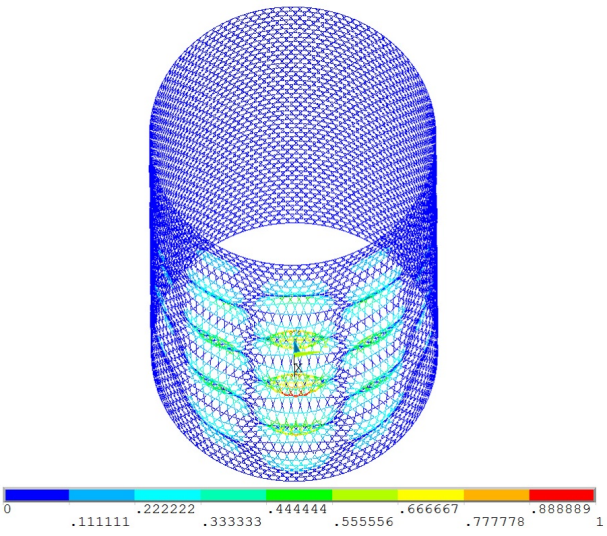


(c)

Figure 9: Buckling failure mode under the action of axial compression force and bending moment (LC3), $\lambda_1 = 1.006$. (a) Front view, (b) and (c) prospective views.

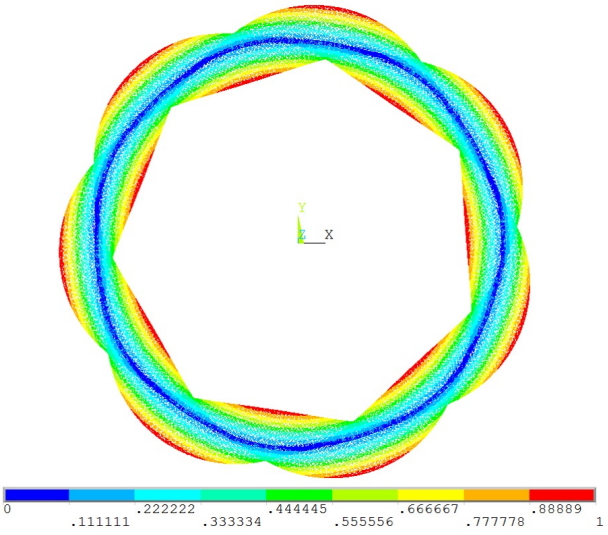


(a)

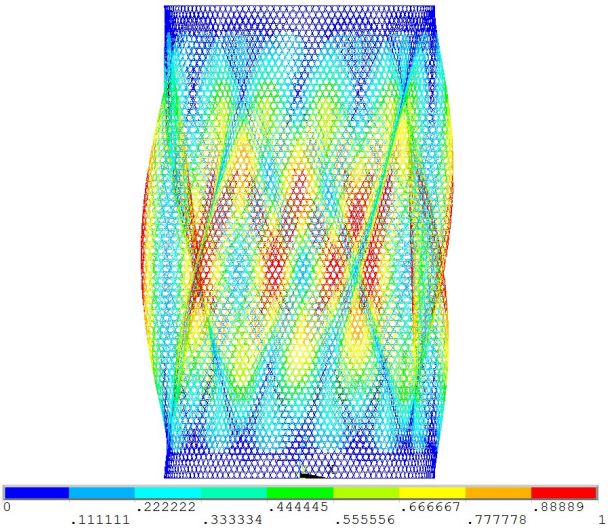


(b)

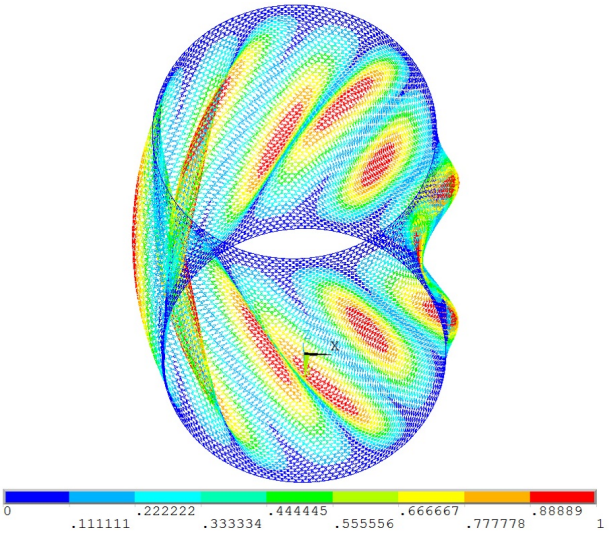


(c)

Figure 10: Buckling failure mode under the action of axial compression force and torque moment (LC4), $\lambda_1 = 1.006$. (a) Top view, (b) front view and (c) prospective view.

*4.4. Torque moment and torsional stiffness constraint (LC4)*

This load case was set up adding a torque moment $T = 3$ MNm (along the $z$ axis of the model) to the simple compression load condition; in addition, a torsional stiffness constraint must be verified as well as the axial one. The torsional stiffness $S_T$ is computed dividing the torque moment $T$ by the rotation $rot_z^{MAX}$ of the upper extremal end about the axis of the lattice shell. A minimum torsional stiffness $S_T = 550$ MNm/rad is required.

The application of the NSGA-II allowed to find out the optimal design parameters reported in Table 7.

This case-study requires a mass increase of 20.22% in reference to the configuration of the initial load case. Moreover, the number of helical ribs $n_h$ and of elementary lattice cells alongside the meridian curve of the shell $N$ are higher. In addition, the cross-section's dimensions of helical and hoop ribs are almost unchanged.

The superposition of the torque moment and the axial force produced an intensification of the maximum compressive axial stress of helical ribs $\sigma_{MAX}$; anyway, it does not reach the compressive strength in fact, the safety factors for this failure mode is 1.41. Contrariwise, the two constraints regarding axial and torsional stiffness and the one about buckling strength of the anisogrid lattice structure are very close to their limit value.

Because of the mixed loading condition here examined, the anisogrid lattice structure buckles according to a buckling failure mode which exhibits 14 oblique stretched lobes alternatively oriented inward and outward with respect to the lattice shell curvature (Fig. 10).

## 5. Comparison between continuous and discrete approaches

The methodology of optimization based on the FE parametric modeling technique in conjunction with the genetic algorithm NSGA-II offers some advantages in respect of the continuous approaches. One of them concerns the capability of providing optimal design solutions for anisogrid lattice structures operating in conditions where different types of load act simultaneously; moreover, any stiffness requirements can be imposed to the lattice shell.

Besides, the continuous approaches present the possibility of inexactly evaluating the critical buckling load of anisogrid lattice structures because the arising of some buckling failure modes is not taken into account by these methods. This can be avoided making use of the proposed method of optimization. In order to further deepen the latter aspect, the numerical results of a sizing problem executed with both methods are presented. The most common optimization technique based on a continuous approach was chosen for this purpose: the minimization of safety factors [5].

The minimization of safety factors is an analytical procedure applicable to anisogrid lattice structures subjected to load cases involving exclusively axial compression, without stiffness requirements, to identify the minimum mass configuration. Because of these features of the analytical method, the anisogrid lattice structure with dimensions and material properties reported in Section 4 is investigated considering only the axial compression load $P = 11$ MN without additional stiffness constraints.

Furthermore, the minimization of safety factors considers three constraint conditions which address compressive strength of helical ribs and resistance to two buckling conditions: global buckling of the shell as a continuum media and in-plane local buckling of helical ribs segments enclosed by two subsequent nodal points, investigated with Euler's formula for columns. This analytical method makes use of four variables: $(I)$ the radial thickness $h$, $(II)$ the angle that the helical ribs form with the meridian curve of the shell $\phi$ and two adimensional values: $(III)$ $\bar{\delta}_h$ and $(IV)$ $\bar{\delta}_c$. The adimensional variables represent the ratio of helical ribs width $\delta_h$ over their spacing $a_h$ and the ratio of hoop ribs width $\delta_c$ over their spacing $a_c$, respectively. The values of the mass $M$ of the optimal configuration and its geometrical variables obtained with this method are listed in Table 8.

Table 8: Design of the anisogrid lattice structure under axial compression with the minimization of safety factors.

| $M$ [Kg] | $h$ [mm] | $\bar{\delta}_h$ [−] | $\bar{\delta}_c$ [−] | $\phi$ [°] |
|---|---|---|---|---|
| 518.9 | 24.10 | 0.0653 | 0.0326 | 26.57 |

Owing to the adimensional variables, it is theoretically possible to find a set of structurally equivalent solutions with different spacings and subsequently diverse number of ribs. Then, the spacing between hoop ribs $a_c$ and helical ribs $a_h$ have to be established to complete the set of geometrical variables and so identify the widths of the ribs. Anyway, the two spacings are not independent, in fact $a_h = 2a_c \sin\phi$, thus it is sufficient to define one of them. In addition, the possible solutions are limited by the technological requirement of realizing an integer number of ribs.

Among the feasible configurations of the lattice shell, three of them were selected to perform the comparison with the results obtained applying the technique of optimization presented in this paper. The configurations were identified establishing a particular value of hoop ribs spacing $a_c$ and consequently of helical ribs spacing $a_h$; following, the widths of the ribs' cross-section were computed and are listed in Table 9.

Finite element models of the three chosen configurations were generated by means of the FE parametric modeling technique and the corresponding values of mass $M$ and angle $\phi$ can be found in Table 9. The slight differences of these values with respect to the analytical ones in Table 8 are due to the necessary rounding of the variables and because the minimization of safety factors considers a configuration of the lattice shell delimited by the overlapping areas between helical ribs, whereas the finite element models were realized choosing the layout with extremal hoop ribs. Anyway, these differences do not influence considerably the structural behavior of the anisogrid lattice structure.

Afterwards, the three identified configurations were verified through finite element analyses (results are reported in Table 9) showing that the anisogrid lattice structure dimensioned with

Table 9: Geometric parameters and finite element analysis results of the anisogrid lattice structure's configurations designed under axial compression with the minimization of safety factors.

| Configuration | $M$ [Kg] | $a_c$ [mm] | $\delta_h$ [mm] | $\delta_c$ [mm] | $\phi$ [°] | $n_h$ | $N$ | $\sigma_{MAX}$ [MPa] | $\lambda_1$ |
|---|---|---|---|---|---|---|---|---|---|
| $(I)$ | 519.6 | 134.6 | 7.86 | 4.39 | 26.65 | 93 | 26 | 349.07 | 0.806 |
| $(II)$ | 519.7 | 112.9 | 6.59 | 3.69 | 26.63 | 111 | 31 | 348.76 | 0.855 |
| $(III)$ | 519.9 | 97.2 | 5.68 | 3.17 | 26.61 | 129 | 36 | 348.13 | 0.893 |

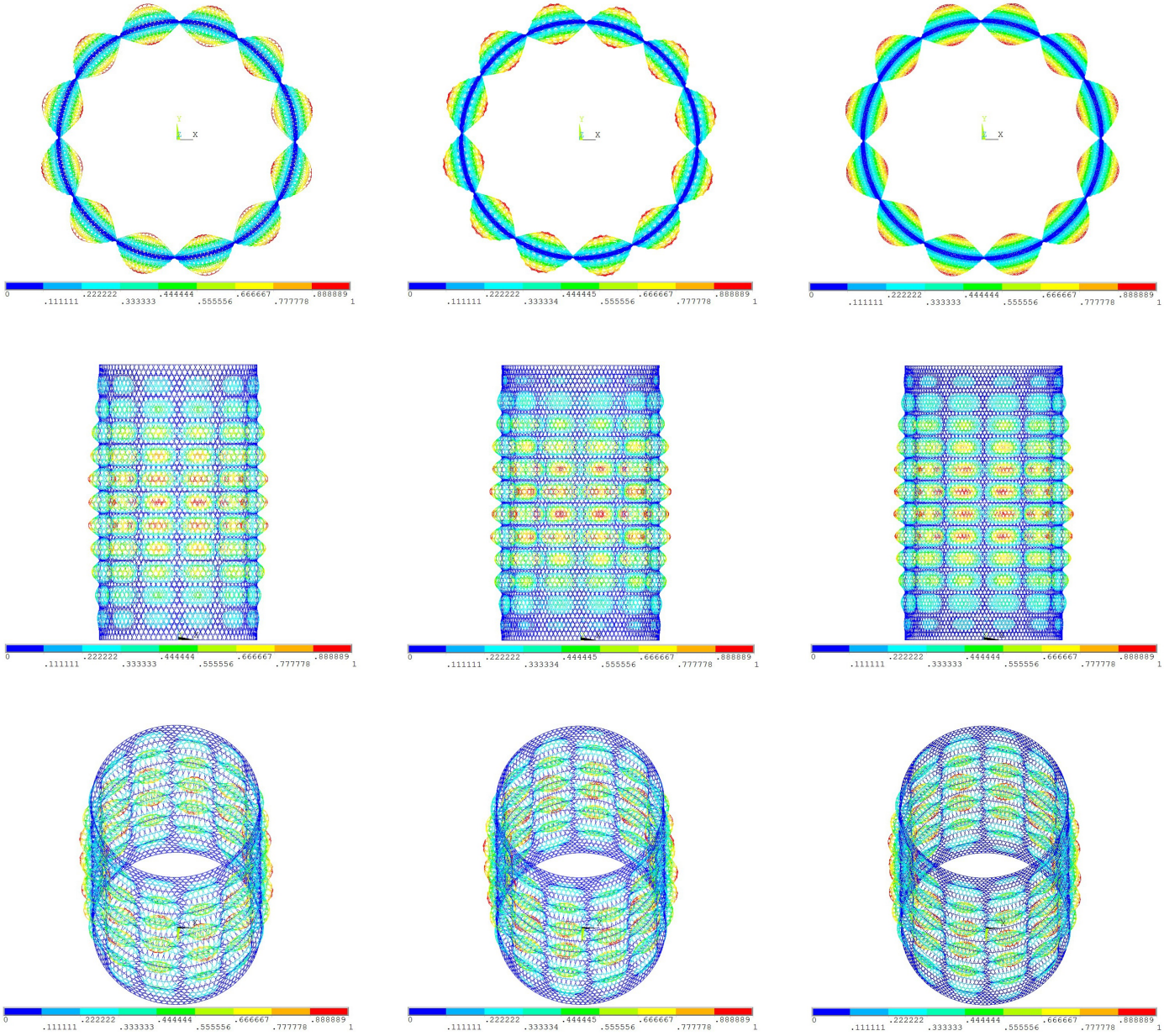

$(I)$ $(II)$ $(III)$

Figure 11: Buckling failure modes under axial compression of the three anisogrid lattice structure's configurations designed with minimization of safety factors. $(I)$ $\lambda_1 = 0.806$, $(II)$ $\lambda_1 = 0.855$, $(III)$ $\lambda_1 = 0.893$

the minimization of safety factors does not resist to the applied compression load. Indeed, the lattice shells obtained from the minimization of safety factors undergoes buckling failure as their first eigenvalues $\lambda_1$, evaluated with finite element analy-

ses, do not reach the unity.

The load-bearing capacity, expressed as critical buckling load, demonstrates an increase with the number of helical ribs $n_h$ passing from the first to the third configuration. Nevertheless, the best load-bearing capacity belongs to the third configuration that buckles for an applied load of about 9.82 MN, i.e. the 10.7% under the value imposed for the design. The reason for the missed fulfillment of the instability constraint is that the buckling failure experienced by the three configurations of anisogrid lattice structure takes place by way of a mode not included in the buckling constraints of the minimization of safety factors, as shown in Fig. 11. For example, the third configuration presents a buckling failure mode featured by 12 series of lobes located around the lattice shell axis and each row consists of 12 lobes arranged in parallel with the lattice shell axis and their amplitude decreases moving towards the extremal hoop ribs.

On the contrary, the application of the design procedure here presented returns an optimal sizing with a mass $M = 525.0$ Kg that satisfies all the constraints, included the one regarding the buckling resistance. The geometrical variables of this configuration are reported in Table 10. Moreover, it should be noted that the inclination angle $\phi$ of the optimum identified by the genetic algorithm differs from the theoretical optimal solution being bigger than that value. The sizing was dominated by the buckling constraint, in fact the first eigenvalue $\lambda_1$ approaches the unity; instead, the safety factor for the compressive stress failure mode is 1.08. The buckling failure mode, reported in Fig. 12, exhibits 10 vertical series of lobes distributed on the circumference, every series is composed of 14 lobes.

Table 10: Geometric parameters and finite element analysis results of the anisogrid lattice structure designed under axial compression with FE parametric modelling and the NSGA-II.

| $M$ [Kg] | $h$ [mm] | $\delta_h$ [mm] | $\delta_c$ [mm] | $\phi$ [°] |
|---|---|---|---|---|
| 525.0 | 26.12 | 4.91 | 3.37 | 31.93 |
| $n_h$ | $N$ | $\sigma_{MAX}$ [MPa] | $\lambda_1$ | |
| 121 | 42 | 417.16 | 1.000 | |

The benefits of an optimization routine with the capability of recognizing all the possible buckling modes that can occur and accordingly sizing the anisogrid lattice structure are relevant. The design solution that it provides does not call for successive adjustments of the lattice structure connected to an overrated failure resistance, this permits to find the true optimal configuration.

## 6. Conclusions

A new methodology for the design and the optimization of anisogrid lattice structures was presented. It overcomes the typical limits of the continuous approaches concerning the incomplete description of the lattice shell buckling modes and the consequent possibility of not satisfying the structural requirements.

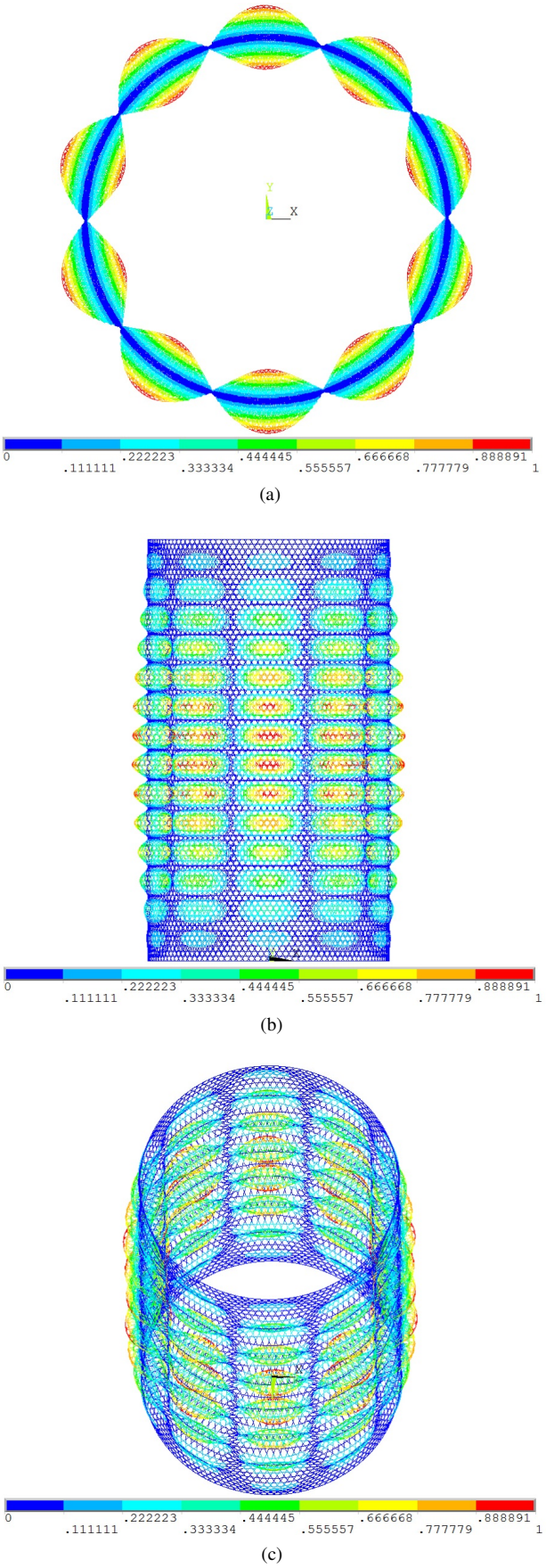


Figure 12: Buckling failure mode under axial compression of the anisogrid lattice structure designed with the FE parametric modelling and NSGA-II, $\lambda_1 = 1.000$. (a) Top view, (b) front view and (c) prospective view.

A versatile parametric FE modeling technique was developed, making use of continuous variables to describe the cross-section dimensions of the unidirectional composite ribs and discrete variables to modify the numbers of helical ribs and of elementary lattice cells alongside the meridian curve of the lattice shell. The proposed method exploits the capabilities of the genetic algorithm NSGA-II which, according to the results of the finite element analysis, manages the input variables of the parametric model to identify the design solution fulfilling all the constraints with the minimum request of mass, i.e. the optimal one.

The design method enlarges the possibilities of optimization of the anisogrid lattice structures encompassing load cases characteristic of the real operative conditions, more complex than the axial compression.

The practical usefulness and applicability to industrial cases was demonstrated through numerical examples where the anisogrid lattice structure was subjected to multiple external loads and stiffness constraints simultaneously applied.

## Acknowledgments

The authors would like to acknowledge Avio Spa for the support to this work.

## References

[1] V. V. Vasiliev, V. Barynin, A. F. Razin, Anisogrid lattice structures survey of development and application, Compos Struct 54 (2001) 361–70.

[2] V. V. Vasiliev, A. F. Razin, Anisogrid composite structures for spacecraft and aircraft applications, Compos Struct 76 (2006) 182–9.

[3] V. V. Vasiliev, V. Barynin, A. F. Razin, Anisogrid composite lattice structures - development and aerospace applications, Compos Struct 94 (2012) 1117–27.

[4] G. Totaro, F. De Nicola, Recent advance on design and manufacturing of composite anisogrid structures for space launchers, Acta Astronaut 81 (2012) 570–7.

[5] V. V. Vasiliev, E. V. Morozov, Advanced mechanics of composite materials and structural elements, Amsterdam: Elsevier, 3rd edition, 2013.

[6] Z. Totaro, Z. Gürdal, Optimal design of composite lattice shell structures for aerospace applications, Aerosp Sci Technol 13 (2009) 157–64.

[7] D. Slinchenko, V. E. Verijenko, Structural analysis of composite lattice shells of revolution on the basis of smearing stiffness, Compos Struct 54 (2001) 341–8.

[8] Q. Zheng, D. Jiang, C. Huang, X. Shang, S. Ju, Analysis of failure loads and optimal design of composite lattice cylinder under axial compression, Compos Struct 131 (2015) 885–94.

[9] E. V. Morozov, A. V. Lopatin, V. A. Nesterov, Finite-element modelling and buckling analysis of anisogrid composite lattice cylindrical shells, Compos Struct 93 (2011) 308–23.

[10] C. Lai, J. Wang, C. Liu, Parameterized finite element modeling and buckling analysis of six typical composite grid cylindrical shells, Appl Compos Mater 21(5) (2014) 739–58.

[11] A. F. Rasin, V. V. Vasiliev, Development of composite anisogrid spacecraft attach fitting, in: Proc. of the 11th European Conf. on Composite Materials, Rhodos, Greece (May 31 - June 3, 2004) CD–ROM, 9 p.

[12] G. Totaro, Local buckling modelling of isogrid and anisogrid lattice cylindrical shells with triangular cells, Compos Struct 94 (2012) 446–52.

[13] G. Totaro, Local buckling modelling of isogrid and anisogrid lattice cylindrical shells with hexagonal cells, Compos Struct 95 (2012) 403–10.

[14] S. Kidane, L. G., J. Helms, S. S. Pang, E. Woldesenbet, Buckling load analysis of grid stiffened composite cylinders, Composites Part B 34 (2003) 1–9.

[15] M. Buragohain, R. Velmurugan, Buckling analysis of composite hexagonal lattice cylindrical shell using smeared stiffener model, Defence Sci J 59(3) (2009) 230–8.

[16] M. Buragohain, R. Velmurugan, Optimal design of lament wound grid-stiffened composite cylindrical structures, Defence Sci J 61(1) (2011) 88–94.

[17] M. Buragohain, R. Velmurugan, Study of filament wound grid-stiffened composite cylindrical structures, Compos Struct 93 (2011) 103138.

[18] L. Sorrentino, M. Marchetti, C. Bellini, A. Delfini, M. Albano, Design and manufacturing of an isogrid structure in composite material: Numerical and experimental results, Compos Struct 143 (2016) 189–201.

[19] E. V. Morozov, A. V. Lopatin, V. A. Nesterov, Buckling analysis and design of anisogrid composite lattice conical shells, Compos Struct 93 (2011) 3150–62.

[20] V. K. Maes, L. Pavlov, S. M. Simonian, An efficient semi-automated optimisation approach for (grid-stiffened) composite structures: Application to ariane 6 interstage, Compos Struct (10.1016/j.compstruct.2016.02.082).